adp

annalen
der physik

Simulation of attosecond-resolved imaging of the plasmon electric field in metallic nanoparticles

James S. Prell[1], Lauren J. Borja[1], Daniel M. Neumark[1,2], and Stephen R. Leone[1,2,3,]*

Sub-cycle photoelectron streaking from silver plasmonic nanospheres is simulated using few-cycle laser pulses tuned both on and off the plasmon resonance (376 nm vs 800 nm, respectively) to initiate the plasmon. Phase-locked, isolated attosecond XUV pulses induce photoemission from the nanospheres, and two different types of streaking of the photoelectrons occur simultaneously due to the laser and plasmon electric fields. Streaking is simulated over a wide range of excitation pulse intensities, and final velocity distributions for the photoelectrons emitted at different times are calculated. The resulting velocity distributions exhibit several characteristics attributable to the plasmon electric field. The dipole moment amplitude can be reconstructed using velocity map imaging or time-of-flight photoelectron velocity measurements without separate measurement of the laser electric field or deconvolution using an assumed streaking trace shape. These results indicate that photoelectron experiments in table-top set-ups can provide unprecedented spatio-temporal information about sub-cycle plasmon dynamics in metallic nanostructures.

1 Introduction

In metal [1] and non-metallic [2, 3] nanostructures, excitation by light at infrared to visible frequencies often produces coherent oscillations of surface charge density on the nanostructure. The dynamics of oscillatory localized surface plasmon resonances (LSPRs), as these excitations are called, depend fundamentally on the electronic properties of the material, and many experiments have demonstrated the remarkable tunability of LSPRs as a function of the compositions [1], shapes, sizes, and dielectric environments of the nanostructures. Plasmonic nanoparticles are important in a broad variety of applications, including surface-enhanced Raman

spectroscopy [4], solar energy production [5], biomedical and chemical sensing [1], and even tumor detection and treatment [6]. The enhanced near field of the plasmon is crucial to many of these applications, as it effectively concentrates the energy of the excitation light field into a very small spatial region, resulting in a stronger interaction with the surrounding chemical environment. The magnitude of the near field enhancement depends strongly on the dephasing time of the LSP oscillation, and a detailed understanding of the factors that lead to plasmon dephasing would be highly useful in designing plasmonic nanostructures for improved signal-to-noise and efficiency in many applications. In this paper, we simulate sub-cycle resolved photoelectron streaking for metal nanoparticles with the goal of isolating effects from the plasmon field. We then suggest experiments that can be used to investigate the build-up and decay of the plasmon electric field on the attosecond timescale including its spatial distribution.

The homogeneous linewidth of an LSPR in a noble metal nanoparticle is inversely proportional to its phenomenological first-order dephasing time, which reflects competing radiative and non-radiative [7, 8] as well as chemical interface damping [9] processes. Measured linewidths for individual silver and gold nanospheres and nanorods fitted using assumed monoexponential decay models indicate a range of dephasing times from approximately one to twelve femtoseconds [7]. The variation of these lifetimes as a function of nanoparticle size, aspect ratio, and overlap of the LSP spectral band with that of interband electronic transitions has been

---

* Corresponding author E-mail: srl@berkeley.edu
[1] Department of Chemistry, University of California, Berkeley, CA 94720-1460, USA
[2] Chemical Sciences Division, Lawrence Berkeley National Laboratory, Berkeley, CA 94720, USA
[3] Department of Physics, University of California, Berkeley, CA 94720-1460, USA

Original Paper

examined in detail [8]. From these experiments, it is evident that radiative damping becomes more dominant with nanoparticle volume and that non-radiative damping due to inelastic electron scattering is faster when the LSPR approaches the resonant frequency for interband electronic transitions. Chemical interface damping is believed to play a significant role only for very small nanoparticles for which the surface-to-volume ratio is very large [9, 10]. Interferometric measurements of second- [11] and third-harmonic [12] generation signals from the surface of nanostructure arrays also indicate low-femtosecond LSP dephasing times. Mie theory [7], the discrete dipole approximation [13], finite-difference time-domain approach [14], and other classical electrodynamics theoretical methods [15] have been used to predict plasmon dephasing times and spectra. These methods typically rely on measurements of the bulk dielectric function of the nanostructure material and do not provide direct information about competing plasmon dephasing processes. In particular, it is unknown under what circumstances plasmon dephasing strictly follows first-order, monoexponential dynamics or when more complicated nonlinear dephasing kinetics occurs, as has been predicted for especially high excitation field intensities [16].

A major hurdle in obtaining more detailed information about the competing processes that lead to these phenomenological dephasing times is the difficulty to directly record subcycle-resolved signals arising from few-femtosecond processes. Over the past decade, isolated light pulses with durations on the order of 100 attoseconds have been generated using the high harmonic method [17–20], and pioneering experiments demonstrating the use of attosecond pulses in probing electron motion in gas-phase atoms [19] and at a metal surface [21] have opened the door to studying few-femtosecond dynamics in a variety of targets. To date, attosecond-resolved dynamics experiments reported in the literature are based on measurements of photoelectron kinetic energies or transient x-ray absorption. Photoelectron streaking [22], in which the momenta of photoelectrons born at a particular time from an atom, molecule, or bulk surface are altered by the surrounding electric field and used to time the birth of the photoelectron, has proven particularly fruitful in measuring few-femtosecond dynamics. This method has only recently been applied to solid samples [21, 23]. Many theoretical studies indicate that the streaking field itself modifies the time evolution of the electron dynamics in the target [24–27]. Evidence for near-field-induced photoelectron acceleration from both metal [28] and insulator [23] nanostructures has been reported, although the oscillation

and decay of the electric field was not resolved in these experiments.

The use of attosecond pulses to resolve few-femtosecond plasmon dynamics has been proposed [29,30], and time-of-flight photoelectron streaking experiments have been simulated for nanospheres [31] as well as coupled nanostructures [32]. Kling and coworkers [31] simulated streaking of photoelectrons in the plasmon electric field of metal nanospheres excited far off-resonance and showed that the kinetic energies of the photoelectrons emitted axially from the nanospheres are closely related to the field amplitude at the poles of the nanospheres. Marangos and coworkers [32] calculated streaking for photoelectrons born between the surface of closely-spaced, coupled nanostructures where the electric field is nearly uniform, and showed that the streaking traces of the photoelectrons collected at a particular angle with respect to the substrate surface to which the nanostructures are attached could be used to recover the amplitude of the electric field between the nanostructures. These investigations show that photoelectron streaking should occur due to the plasmon electric field using few-femtosecond laser pulses to initiate the plasmon and phase-locked isolated attosecond pulses to eject the electrons. However, a general method for use with a variety of nanoparticle shapes and sizes excited on- or off-resonance has heretofore not been reported.

In order to measure the dynamics of plasmon build-up and decay in the nanoparticles via streaking, it is necessary to determine how the envelope of the plasmon dynamical dipole moment amplitude can be reconstructed from the photoelectron streak trace subject to the limitations of available photoelectron detection technology. In this paper, we calculate the photoelectron streaking due to the oscillatory electric field of LSPs for silver nanospheres irradiated with light that is either on- or off-resonance, with photoemission timed by an isolated attosecond pulse with a specific band of photon energies. The final velocity distribution after streaking is shifted by the laser field, and the plasmon electric field causes the shape of the velocity distribution to become distorted, broadened, and anisotropic. We illustrate how these plasmonic streaking properties can be exploited to reconstruct the dipole moment amplitude build-up and dephasing directly using either velocity map imaging [33] or time-of-flight measurements without the need for separate measurement of the laser for either case. Velocity map imaging has not previously been investigated in depth as a probe of plasmon dynamics, and we infer several benefits of using this technique in addition to time-of-flight. These results indicate that

Original Paper

well-established methods in photoelectron spectroscopy, together with few-cycle, phase-locked lasers and isolated attosecond pulse production, can provide sub-cycle resolution of dephasing dynamics in plasmonic nanostructures.

2 Computational methods

Sub-cycle plasmon dynamics in silver nanospheres excited with few-fs laser pulses are simulated using linear response theory, and streaking of photoelectrons emitted with phase-locked, isolated XUV attosecond pulses is calculated using classical electrodynamics. The electric field of localized surface plasmons is simulated for silver nanospheres with a diameter of 80 nm excited with a 5 fs, Fourier transform-limited plane wave laser light field at 376 (resp., 800) nm traveling in the x-direction with the electric field polarized along the z-direction. Light at these wavelengths can be focused to a beam waist on the order of a hundred microns and a peak intensity of 10^{13} W/cm^2 or higher with relative ease.

In the quasi-static approximation, the linear response of the plasmon, characterized by its dynamical dipole moment, $p(t)$, to the electric field of an incident (inc) excitation pulse polarized in the direction of the unit vector $\vec{z}$, $\vec{E}_{inc}(t) = \vec{z}E_{inc}(t)$, determines the temporal evolution of the plasmon electric field as a function of time according to the following equations:

$$\tilde{p}(\omega) = \epsilon_0 \tilde{\alpha}(\omega) \tilde{E}_{inc}(\omega) \tag{1}$$

$$\tilde{p}(t) = \vec{z} p(t) \equiv \vec{z} \, IFT(\tilde{p}(\omega)) \tag{2}$$

where ε_0 is the permittivity of free space, $\tilde{\alpha}(\omega)$ is the complex polarizability of the nanosphere, $\tilde{E}_{inc}(\omega)$ is the complex Fourier transform of the incident laser electric field, and IFT is the inverse Fourier transform operation. The complex polarizability is modeled using Mie theory to second order in the size parameter $x = \frac{\pi(40\,\text{nm})}{\lambda_0}$ [34]. The dynamical dipole moment response of the nanospheres in vacuum to either an impulse excitation or a transform-limited resonant ($\lambda_0 = 376$ nm) or off-resonant $\lambda_0 = 800$ nm), 5 fs laser pulse is modeled classically using experimental refractive index data [35]. The spatial distribution of the electric field of the plasmon is then [36]

$$\vec{E}_{pl}(\vec{n}, t) = \frac{1}{4\pi \varepsilon_0} \left\{ k^2 (\vec{n} \times \vec{p}(t)) \times \frac{\vec{n} e^{ikr}}{r} \right.$$
$$\left. + [3\vec{n}(\vec{n} \cdot \vec{p}(t)) - \vec{p}(t)] \left(\frac{1}{r^3} - \frac{ik}{r^2} \right) e^{ikr} \right\} \tag{3}$$

In this equation, k is 2π times the wavenumber of the incident electric field, and $\vec{n}$ is the unit position vector for a point located at a distance r from the center of the nanosphere. The term on the right hand side of Equation (3) that is proportional to r^{-3} dominates within a few tens of nanometers of the nanosphere and represents the near field. Inside the nanosphere, boundary conditions require that the electric field is uniform and equal in direction and magnitude to the value of the electric field at the nanosphere surface where $\vec{n}$ is perpendicular to $\vec{z}$, i.e., along the "equator" of the nanosphere.

The trajectories of photoelectrons emitted from the nanospheres using isolated attosecond XUV pulses are simulated classically. Isolated attosecond light pulses centered near 50 eV and having a duration of approximately 140 attoseconds can be generated using the high harmonic method [18], and the delay between the XUV pulse and the infrared pulse used to create it can be controlled using a split mirror or interferometer. In order to cover the broad range of photoelectron energies that can be accessed with isolated attosecond pulses using current technology, the trajectories of point-like photoelectrons created with initial energies of precisely 10, 50 and 90 eV are simulated. The finite ($\sim$13 eV) bandwidth of the 140 attosecond pulse will result in a distribution of initial kinetic energies that can be deconvolved experimentally when the dependence of the streaking on initial kinetic energy is small over the bandwidth sampled, as is the case in our simulations. Using tightly focused XUV light generated by the high harmonic method and a weakly focused incident pulse, the beam waist of the XUV light can be significantly smaller than that of the 376 nm or 800 nm excitation pulse (Figure 1, top). The magnitude of the laser and plasmon electric fields as a function of the position of the nanosphere within the photoelectron probe volume will therefore not vary significantly. No such variations are explicitly included in the simulations.

The location of the birth of the photoelectrons is sampled uniformly within 3 mean free path lengths of the surface of the nanosphere, and the initial direction of travel for the photoelectrons is sampled isotropically. Candidate trajectories are accepted based on their relative probability of escape $\exp\left(-\frac{d}{d_{mfp}}\right)$, where d represents the distance the photoelectron must travel to the surface of the nanosphere in the direction of its initial velocity and d_{mfp} is the mean free path of the electrons ($\sim$0.5 nm over the entire range of initial kinetic energies investigated) [37]. Effectively, this weighting favors electron trajectories traveling radially outward from the nanosphere and discriminates strongly against trajectories directed toward the interior of the nanospheres.

One million trial photoelectrons are generated at each delay time in order to sample the full space of possible initial positions and velocity directions. Classically,
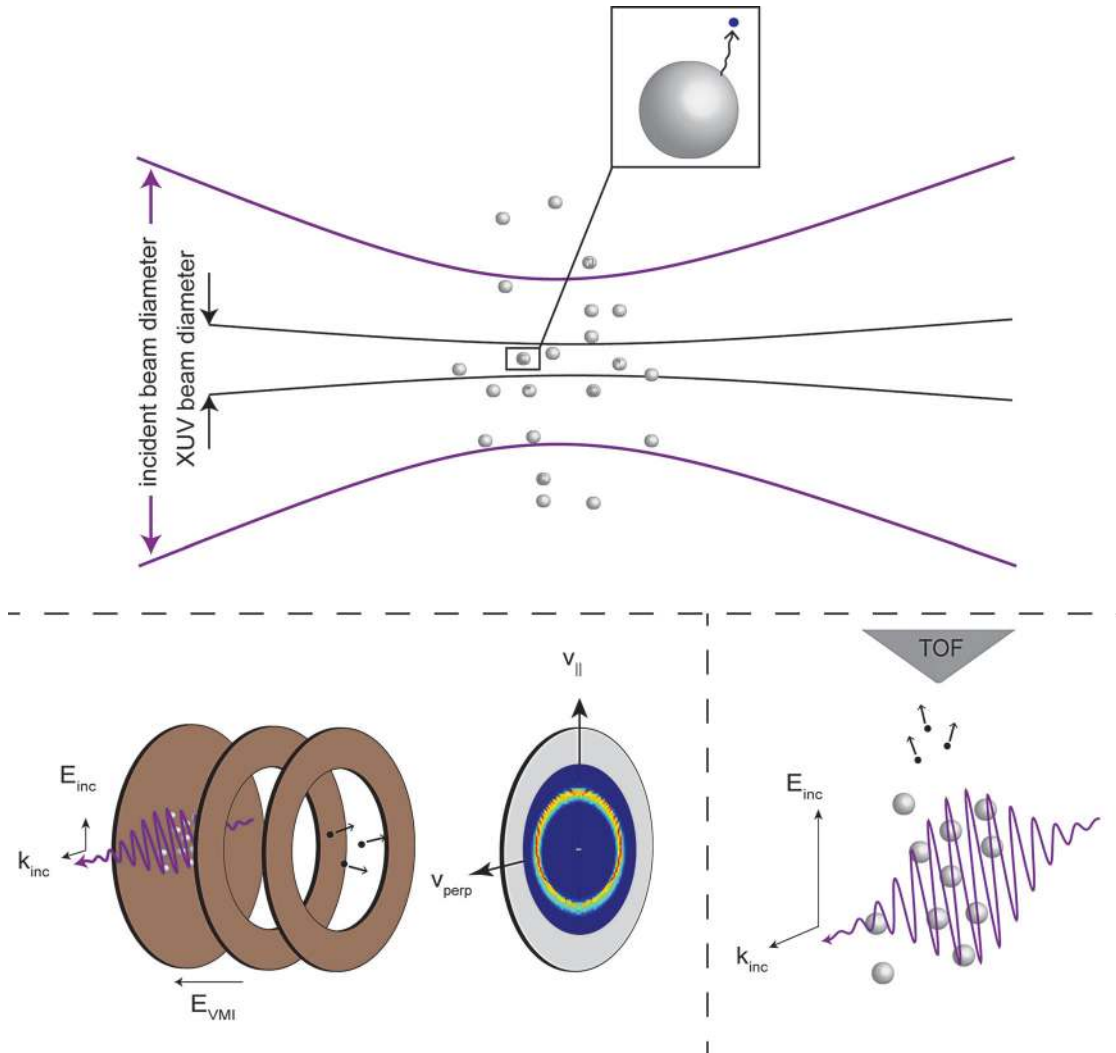
Figure 1 (online color at: www.ann-phys.org) Schematics of proposed experiments for observing localized surface plasmon dynamics in metal nanospheres. Top: illustration of interaction region; inset shows trajectory of a photoelectron streaked by the laser and plasmon electric fields. Bottom: experimental geometry for velocity map imaging (left) and time-of-flight electron spectrometer. E_{inc} and k_{inc} represent the electric field polarization direction and propagation direction of the incident laser that excites the plasmon, respectively, E_{VMI} indicates the direction of the electrostatic field of the VMI apparatus, and $v_{||}$ and v_{perp} indicate photoelectron velocity directions parallel and perpendicular to E_{inc}, respectively.

the final velocity of each electron is given by

$$\vec{v}_f = \vec{v}_i - \frac{e}{m_e} \int_{t_{birth}}^{\infty} \vec{E}_{tot}(\vec{r}(t))\,dt \qquad (4)$$

where $\vec{v}_i$ and $\vec{v}_f$ are the initial and final velocities of the electron, e and m_e are the charge and mass of an electron, t_{birth} is the time at which the photoelectron is created, and $\vec{E}_{tot}(\vec{r}(t))$ is the total electric field (plasmon plus laser). (The temporal center of the incident pulse is defined as $t_{birth} = 0$.) Trajectories are numerically integrated here in 10 attosecond increments for a total of 50 fs. This assures that the momentum of the photoelectrons is no

longer being changed significantly by the laser and plasmon electric fields at the time the trajectories are terminated.

3 Results and discussion

3.1 Plasmonic photoelectron streaking

Figure 1 illustrates the interaction region (top) and apparatus geometries for the two types of photoelectron experiments (bottom left: velocity map imaging, bottom right: time-of-flight electron spectrometry) modeled

here. Briefly, a localized surface plasmon is initiated with a 5-fs, 376 nm or 800 nm laser pulse. A photoelectron is then emitted using an attosecond XUV pulse, and the photoelectron traverses the field inside the nanosphere before escaping the surface with a probability dependent on the inelastic mean free path for electrons in silver ($\sim$0.5 nm [37]). If the photoelectron escapes the nanosphere, it is streaked by both the laser and plasmon electric fields until these fields vanish, and the resulting distribution of photoelectron final velocities acts as a record of the electric field experienced by the photoelectrons during this process. The repetition rate of lasers currently used to produce 5-fs pulses is typically on the order of one to several kilohertz, thus an aerosolized beam of nanospheres will traverse the interaction completely between pulses, refreshing the sample. Although photodamage to the nanospheres may occur at intensities above 10^{12} W/cm^2, it will occur on the timescale of phonon propagation, which is unimportant to the much faster photoelectron motion investigated in these simulations.

The plasmon response to a 5 fs, 376 nm or 800 nm laser pulse with peak intensity 10^{12} W/cm^2 is simulated as described above using experimental refractive index data [35] and is shown in Figure 2. As expected, the response to the on-resonance pulse is approximately one quarter of an optical cycle out of phase with the incident pulse and has an exponentially decaying tail at times after the peak of the incident pulse. By contrast, the response to the off-resonance pulse is in phase with the incident pulse and is weaker than the on-resonance response. Streaking of photoelectrons emitted by XUV photons from resonantly excited nanospheres is illustrated in Figure 3, where a slice through the final photoelectron velocity distribution is shown for several values of t_{birth} near the time at which the plasmon response is maximal (see Fig. 2). The photoelectrons in Fig. 3 have an initial kinetic energy of 50 eV, much higher than that of any secondary electrons or photoelectrons produced through multiphoton photoemission by the incident (376 nm or 800 nm) pulse. The images in Fig. 3 are related to what would be observed in a VMI experiment, as discussed in more detail below.

Several features of the final velocity distributions that evolve in time are revealed beyond those expected from traditional gas-phase streaking experiments, and these new features are attributable to the presence of the plasmon field (Fig. 4). Streaking of the entire distribution up and down along the laser polarization axis by the laser electric field is observed, but the final velocity distribution is also periodically distorted and broadened from its isotropic (spherical) shape at the time of birth of the
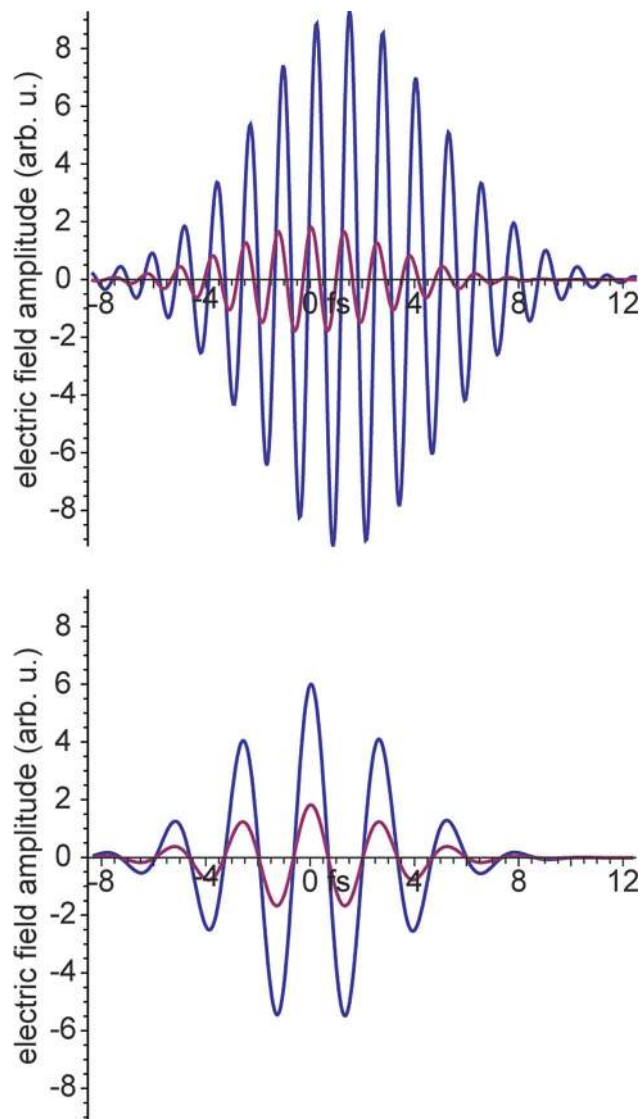

Figure 2 (online color at: www.ann-phys.org) Total electric field (high-amplitude purple line) at the apex of a silver nanosphere with 80 nm diameter calculated using Mie theory and refractive index data from Palik [35] to a linearly polarized 5 fs, transform-limited resonant (376 nm; top, magenta line) or off-resonant (800 nm; bottom, magenta line) laser pulse.

photoelectrons, and there is modulation of the photoelectron angular distribution along the laser polarization axis ($\vec{v}_{||}$). These features can be explained by noting that photoelectrons that acquire final velocities, $\vec{v}_f$, in a given direction can originate from a broad region of the nanosphere, $R(\vec{v}_f)$, as illustrated in the middle of Fig. 4. In contrast to the laser field, the plasmon electric field is highly anisotropic, so the electrons are streaked by different amounts depending on where they exit the nanosphere. Because the magnitude of streaking is
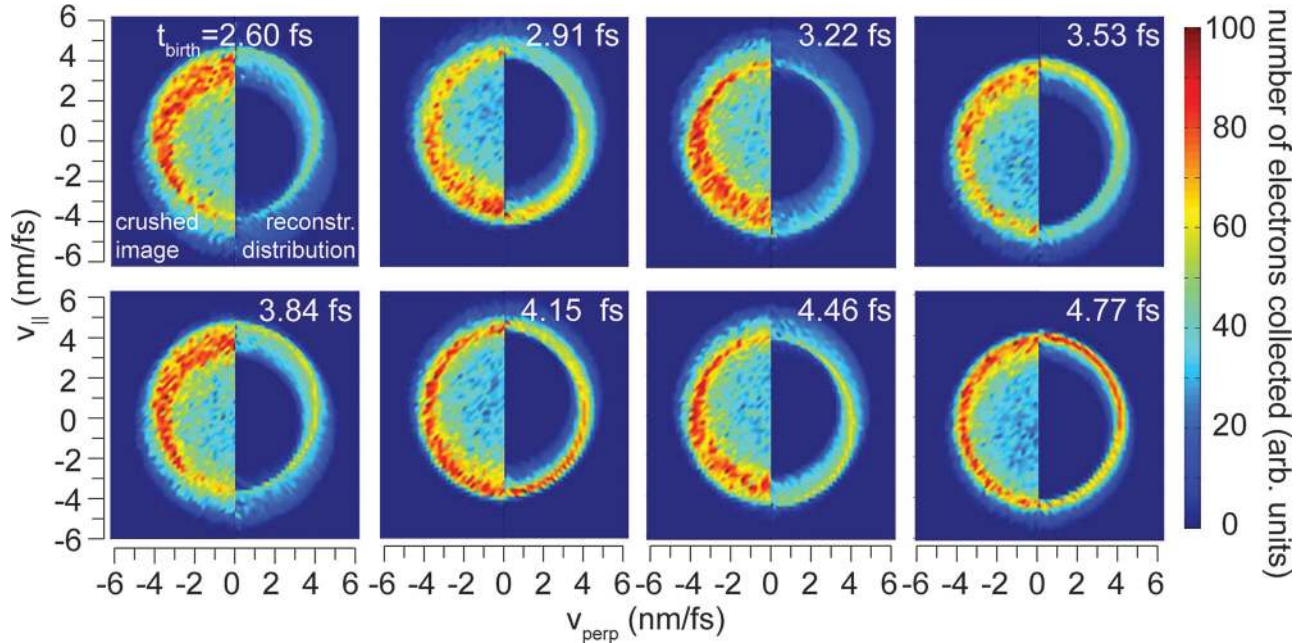
Figure 3 (online color at: www.ann-phys.org) Simulated photoelectron streaking from silver nanospheres with 80 nm diameters using a 5 fs, transform-limited resonant (376 nm) laser pulse with peak intensity 10^{13} W/cm^2. The initial kinetic energy of the electrons in this simulation was 50 eV, and the color bar on the right side of the figure indicates the relative density of photoelectrons collected with a given velocity in a plane parallel to and containing the polarization direction of the plasmon (the same scaling is used for each velocity-space image). "Crushed" velocity map images are shown on the left in each frame, and reconstructed central slices through the 3-dimensional final velocity distribution are shown on the right. These images are taken for t_{birth} near the maximum of the dynamical plasmon dipole moment response (see Fig. 2). Typical up-down oscillation along the laser polarization axis ($\vec{v}_{||}$) due to laser streaking as well as an oscillatory broadening, shape distortion, and intensity gradient attributable to the plasmon electric field are present. These features can be used to reconstruct the dynamical plasmon dipole moment (see text).

small compared to the initial velocities of the photoelectrons over the range of parameters investigated here, the direction of streaking for most photoelectrons with final velocity $\vec{v}_f$ is well represented by the direction of the electric field at the location on the nanosphere surface where these photoelectrons exit. This accounts for the calculated distortion and broadening of the final velocity distribution. Depending on the direction of $\vec{v}_f$, the plasmonic streaking can cause either a net convergence or divergence of trajectories for photoelectrons with final velocity $\vec{v}_f$ (Fig. 4, top), leading to a photoelectron flux that depends on the angle between $\vec{v}_f$ and the $\vec{v}_{||}$ axis. This results in the calculated intensity gradient that varies along the $\vec{v}_{||}$ axis.

3.2 Velocity map imaging for reconstruction of the plasmon dipole moment

All of the above mentioned features of the photoelectron final velocity distribution can in principle be measured experimentally using velocity map imaging (VMI),

a technique that is used to reconstruct the final velocity distributions of photoelectrons in streaking experiments, such as those shown in Fig. 3. In VMI, the final distribution of photoelectrons ejected from a gas or nanoparticle jet after streaking by an electric field is "crushed" onto an imaging detector parallel to the polarization axis using electrostatic fields (Fig. 1, bottom left). Under appropriate experimental conditions, photoelectrons with the same streaked final velocity component in the plane parallel to the detector are mapped to the same point on the detector, independent of the target particle from which they originated. From the "crushed" velocity map image (Fig. 3, left-hand side of each frame), the distribution of final electron velocities can be reconstructed using computer algorithms (Fig. 3, right-hand side of each frame).

Of the three features described above that are caused by plasmonic streaking (shape distortion, broadening, and modulation of the photoelectron angular distribution along the $\vec{v}_{||}$ axis), it is expected that broadening and the intensity gradient will be the most readily measurable under realistic experimental conditions.
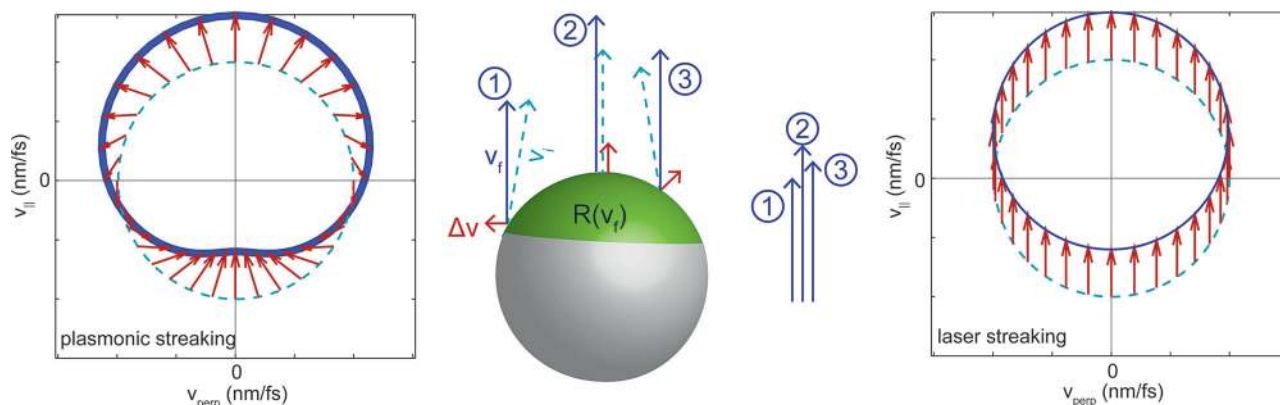
Figure 4 (online color at: www.ann-phys.org) Schematic illustration of plasmonic (left) and laser (right) streaking of photoelectrons from a nanosphere. In velocity space, the photoelectron velocity is isotropic (left, dashed blue line) at the time of birth of the photoelectrons, but plasmonic streaking causes distortion of the velocity distribution to a more flattened shape (thick purple line) that is significantly broadened due to the range of final velocities attained for electrons born at different locations within $R(\vec{v}_f)$ for each $\vec{v}_f$. The origin of the broadening is illustrated in the middle panel for three photoelectrons that escape the nanosphere in different directions with the same initial speed but acquire final velocities, $\vec{v}_f$ (numbered arrows), along the same direction. These electrons originate from different locations over a large region of the nanosphere, $R(\vec{v}_f)$, and their initial velocities ($\vec{v}_i$, dashed blue arrows) are streaked in different directions by different amounts, $\Delta\vec{v}$ (red arrows) that depend on the direction and magnitude of the plasmon electric field where they exit the nanosphere. Although their final velocities all lie along the same direction, they have different final speeds. This contrasts with traditional gas-phase streaking (right), in which the initial velocity distribution shifts as a whole up and down the laser polarization (vertical) axis.

The breadth of the distribution can be measured using the standard deviation in the photoelectron final velocity distribution, averaged over all final velocity directions θ to yield an experimental observable, $\langle\sigma(v_f)\rangle_\theta$. This quantity as a function of photoelectron emission time, t_{birth}, is shown in Figure 5 (red lines) for a resonant (top, 376 nm) and off-resonant (bottom, 800 nm), 5 fs laser pulse with intensity 10^{12} W/cm^2 along with the simulated dynamical plasmon dipole moment amplitude, $p(t)$. The magnitude of $\langle\sigma(v_f)\rangle_\theta$ closely reproduces the envelope of the dipole moment amplitude (Fig. 5, green lines), oscillates at twice the frequency of the plasmon, and its local maxima occur one quarter of an optical cycle out of phase with the peaks and troughs of $p(t)$. The doubled frequency with respect to $p(t)$ occurs because the range of electric fields over any given surface region $R(\vec{v}_f)$ oscillates at twice the plasmon frequency, and the phase delay occurs as expected from the integration in Equation (4). A proportionality constant for $\langle\sigma(v_f)\rangle_\theta$ versus the peak laser electric field amplitude of $\sim$0.85 nm/(fs V Å^{-1}) can be derived from these results, but we caution that this value in an experiment will depend on the size of $R(\vec{v}_f)$, which may not be accurately modeled in our simulations. The noise in Fig. 5 that is most obvious at especially early and late t_{birth} is a computational artifact at-

tributable to imperfect isotropy of the simulated initial photoelectron velocity distribution.

Under these simulation conditions, the magnitude of $\langle\sigma(v_f)\rangle_\theta$ varies linearly with the laser peak electric field strength for peak intensities from $10^{10} - 10^{13}$ W/cm^2 and is nearly independent of the initial photoelectron kinetic energy from 10 eV to 90 eV. Thus, the additional breadth in the initial photoelectron kinetic energy distribution due to the finite bandwidth ($\sim$13 eV) and duration of the 140 attosecond XUV pulse causes no significant change in the plasmon streaking effects, and the measured standard deviation in the initial photoelectron speed in the absence of laser or plasmon fields can be subtracted in quadrature from $\langle\sigma(v_f)\rangle_\theta$ to recover $p(t)$. This recovery does not require separate measurement of streaking by the laser pulse alone and should be readily achievable with available velocity map imaging technology using an aerosolized beam of nanospheres of uniform size [38]. Based on these simulations, a momentum resolution of approximately 2% for a VMI device is required to reconstruct the dynamical plasmon dipole moment amplitude at an incident pulse intensity of 10^{11} W/cm^2, and resolution exceeding this value has recently been demonstrated in gas-phase VMI experiments using attosecond XUV pulses [39].
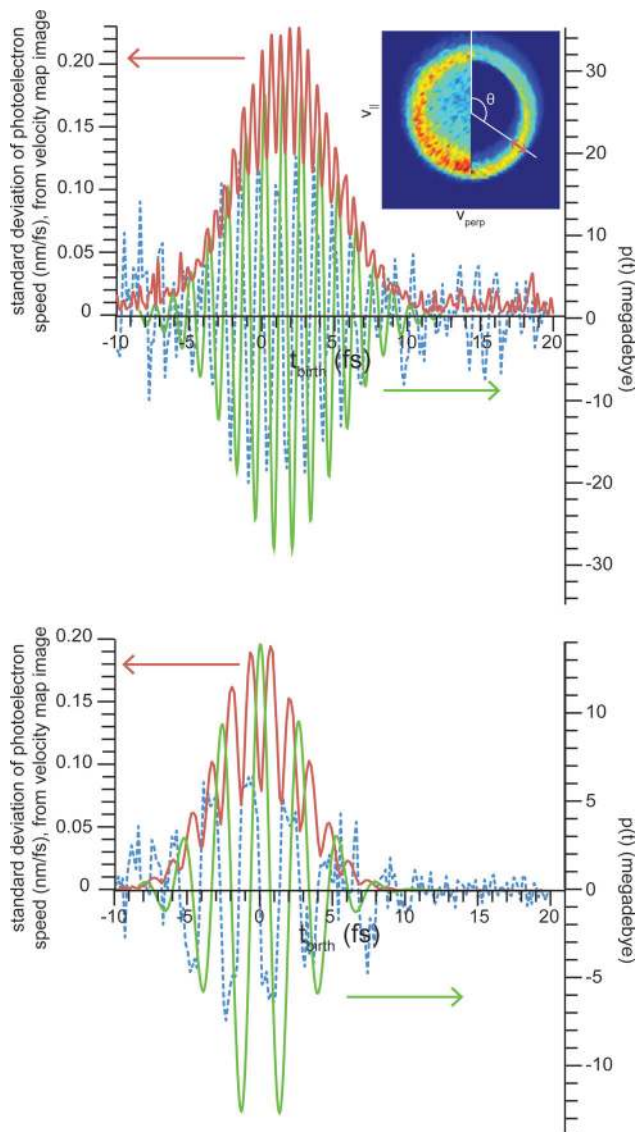
Figure 5 (online color at: www.ann-phys.org) Plot of the breadth of the photoelectron final velocity distribution, $\langle \sigma(v_f) \rangle_\theta$ (see text for definition), versus t_{birth} (red, left axis) and plasmon dynamical dipole moment amplitude (green, right axis) under the same conditions as in Fig. 2, but with a laser peak intensity of 10^{12} W/cm^2 and wavelength 376 nm (top) and 800 nm (bottom). As shown in the inset, θ is the angle between the photoelectron final velocity and the laser polarization direction, and $\langle \sigma(v_f) \rangle_\theta$ is the average over all θ of the breadth illustrated by the red double-headed arrow. Blue dotted lines indicate the relative contribution (arbitrary units) of the Legendre polynomial $P_1(\cos\theta)$ to the final velocity distribution.

The intensity gradient of the final velocity distribution can be analyzed with a multipole decomposition of the velocity map images using Legendre polynomials, $P_n(\cos\theta)$), as is often done in conventional VMI. Under the range of conditions investigated here, only P_0 and

P_1, which represent isotropic and top-bottom asymmetric distributions, respectively, contribute significantly to the calculated velocity distributions, consistent with the strong monotonic intensity gradient along the $\vec{v}_\parallel$ axis. The relative magnitude of the P_1 contribution as a function of t_{birth}, which reports the magnitude of the oscillating intensity gradient, is shown (dotted blue lines) in Figure 5. Evidently, this metric reconstructs $p(t)$ with a quarter-cycle phase delay, but it is somewhat noisier than $\langle \sigma(v_f) \rangle_\theta$. In both of these methods, all of the photoelectrons emitted from the nanospheres are collected and used to reconstruct the dynamical plasmon dipole moment. For nanostructures, such as nanorods, that support plasmons with much greater variation of the plasmon electric field across the nanostructure surface, even greater distortion of the final velocity distribution should be observed. Due to the position-velocity correspondence between $R(\vec{v}_f)$ and $\vec{v}_f$, the angle-dependent distortion observed with VMI should provide spatial information about the electric field distribution for such nanostructures.

3.3 Time-of-flight reconstruction of the plasmon dipole moment

As an alternative to VMI, a time-of-flight electron spectrometer could be used experimentally to measure the photoelectron speed distribution collected within some small cone angle about the polarization axis of the nanospheres. The simulated photoelectron streaking trace from a time-of-flight device with a 30 degree (full cone) acceptance angle is shown in Figure 6, including the finite (13 eV) bandwidth and duration of the 140 attosecond pulse. The plasmon field-induced standard deviation $\sigma(v_f)_{TOF}$ in the speed of the photoelectrons about the primary photoelectron peak can then be calculated and plotted as a function of delay time, as shown in Figure 7. This method can be used to reconstruct $p(t)$, and although the modulation depth is lower than that for velocity map imaging, and signal to noise is better for time-of-flight. The lower modulation depth of the oscillations in $\sigma(v_f)_{TOF}$, which is important for reconstructing the phase of $p(t)$, arises from the uncertainty in the angle of the photoelectron velocities relative to the polarization axis. Using a smaller collection cone angle for the time-of-flight results in a nearly identical trace for $\sigma(v_f)_{TOF}$ that has greater modulation depth but smaller amplitude due to the smaller number of collected electrons. Thus it may be advantageous experimentally to strike a balance between having as small a collection angle as possible with sufficient photoelectron counts
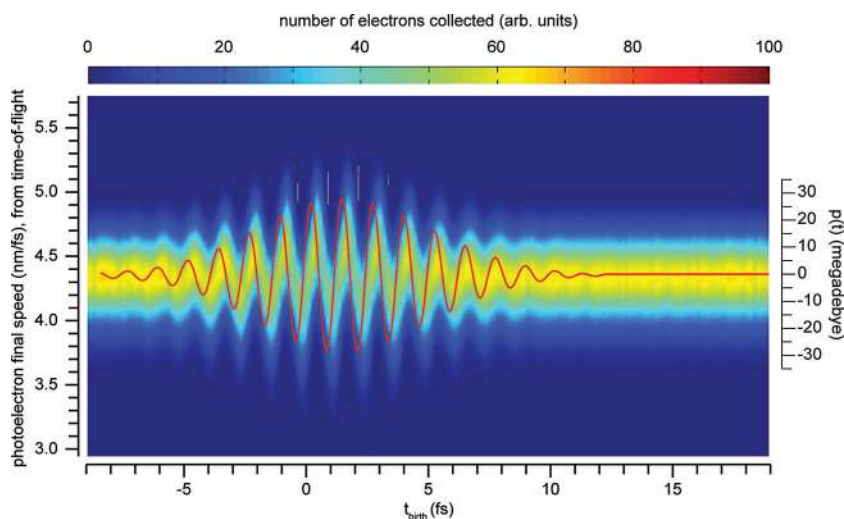
Ann. Phys. (Berlin) **525**, No. 1–2 (2013)

annalen
der **physik**

Original Paper

Figure 6 (online color at: www.ann-phys.org) Simulated final speed distribution for photoelectrons streaked from silver nanospheres under the same excitation conditions as in Fig. 5, as measured using a time-of-flight with a 30° full cone collection angle about the plasmon polarization axis. Blurring of the streaking trace due to the 140 attosecond duration and 13 eV energy bandwidth of the initial photoelectron distribution is included, and the plasmon dynamical dipole moment amplitude (red line, right axis) is shown for comparison.
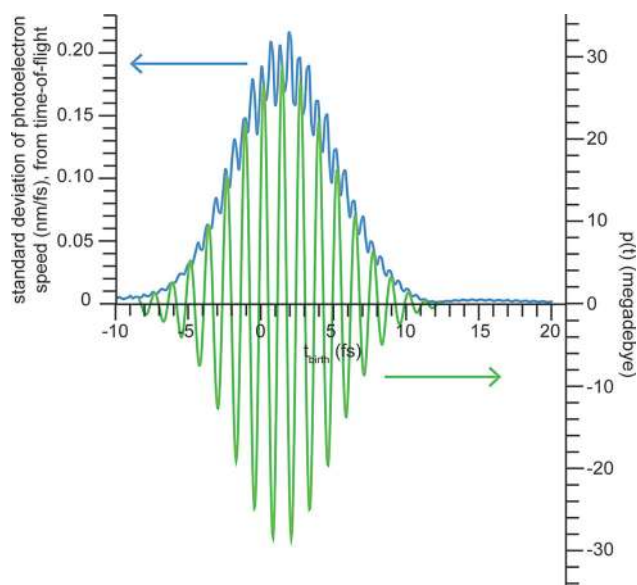
Figure 7 (online color at: www.ann-phys.org) Plot of the standard deviation in speed measured using an electron time-of-flight with a 30° full cone collection angle about the plasmon polarization axis, $\sigma(v_f)_{TOF}$, versus t_{birth} (blue, left axis) and plasmon dynamical dipole moment amplitude (green, right axis) under the same conditions as in Fig. 5, top.

to be able to obtain the best quality plasmon dipole moment amplitude reconstruction from time-of-flight spectra.

In many time-of-flight streaking experiments, the average photoelectron speed is used to characterize the streaking field, rather than the breadth of the streak trace, as described above. Because the photoelectrons collected in a time-of-flight spectrometer such as the one modeled here originate from a large region on the

nanosphere over which the plasmon electric field is strongly inhomogeneous, the average speed measured in the time-of-flight streaking trace cannot be simply decomposed into contributions from the laser and plasmon electric fields. The effects of the laser and plasmon electric fields are nearly additive under the conditions investigated here (see above), but the precise ratio of the laser peak electric field amplitude to the peak plasmon dipole moment amplitude may be difficult to establish experimentally without precise characterization of the region from which the collected photoelectrons originate. Although it is tempting to conclude that the average speed in the time-of-flight streaking trace reproduces the total electric field envelope at some point(s) on the nanosphere, it is challenging to determine *which* point(s) without precise characterization of $R(\vec{v}_f)$, the region of the nanosphere from which the collected photoelectrons originate. Within the limits of our simulations, it is clear that this point is not the apex of the nanosphere, and that reconstruction of $p(t)$ using $\sigma(v_f)_{TOF}$ is much more direct.

4 Conclusions

This paper models possible experiments where an attosecond light pulse is used to eject electrons from a metal nanosphere in which a plasmon has been excited by a few-cycle optical pulse. Classical simulations for the emitted photoelectrons indicate that the streaking of the photoelectrons by the electric fields of the optical laser pulse and the induced plasmon dynamical dipole moment in the nanosphere can be observed under ultrahigh vacuum conditions using electron time-of-flight and velocity map imaging measurements for laser peak

intensities below $\sim 10^{13}$ W/cm^2. The action of the (homogeneous) laser field in the photoelectron final velocity distributions is associated primarily with translation of the entire distribution up and down the axis parallel to the plasmon dipole moment, and the strongly inhomogeneous plasmon field distorts and broadens the distribution as well as causing an intensity gradient of the photoelectrons along the polarization axis. These effects scale approximately linearly with peak laser electric field amplitude and depend only weakly on initial photoelectron kinetic energy over the range of kinetic energies investigated here.

The wide distribution of angles with respect to surface normal at which the photoelectrons can escape the nanostructure surface results in a correlation between the final electron velocity direction and the region of the nanostructure from which it originates. This property arises on the nanoscale because the inelastic mean free path (~ 0.5 nm) of the primary photoelectrons inside the nanostructures is very small compared to the dimensions of the nanostructures. This correlation is useful for reconstructing not only the build-up and decay of the plasmon electric field in time, but also its spatial distribution. Velocity map imaging may be ideal to measure directly the temporal build-up and decay of the plasmon dipole moment amplitude for monodisperse nanospheres or aligned non-spherical nanostructures with attosecond temporal resolution and sensitivity to nanostructure aspect ratio and orientation.

This ability to measure the plasmon dynamical dipole moment directly, without the need for deconvolution of the laser field contribution and a modeled plasmon response, could prove especially useful under conditions where the plasmon response is nonlinear or damps according to kinetics not explored here. For example, a recent computational study has shown that plasmon excitation by an especially strong laser field may lead to multiphoton or tunneling photoemission that induces dynamic contraction of the free electron cloud and slower damping [16]. The correlation in these simulations between initial photoelectron velocity and the region of the nanostructure from which the photoelectron originates could also be advantageous for investigating energy flow between coupled plasmonic nanostructures. For nanostructures with large aspect ratios, more photoelectrons will originate from flatter regions of the nanostructure than from more curved regions, so it should be possible to follow streaking for the especially high density of photoelectron velocities corresponding to emission from the flattest portion of the surface. The streaking of this "rainbow angle"-like feature in the ve-

locity map image could be used to obtain unprecedented spatio-temporal information about the plasmon electric field distribution at the surface of a variety of nanostructures or to map energy transfer between adjacent nanostructures with different shapes.

References

[1] P. K. Jain, X. H. Huang, I. H. El-Sayed, and M. El-Sayed, Acc. Chem. Res. **41**, 1578–1586 (2008).
[2] J. M. Luther, P. K. Jain, T. Ewers, and A. P. Alivisatos, Nature Mat. **10**, 361–366 (2011).
[3] M. Kanehara, H. Koike, T. Yoshinaga, and T. Teranishi, J. Am. Chem. Soc. **131**, 17736–17737 (2009).
[4] G. V. P. Kumar, J. Nanophotonics **6**, 064503 (2012).
[5] C. Hägglund, M. Zäch, G. Petersson, and B. Kasemo, Appl. Phys. Lett. **92**, 053110 (2008).
[6] A. M. Gobin, M. H. Lee, N. J. Halas, W. D. James, R. A. Drezek, and J. L. West, Nano Lett. **7**, 1929–1934 (2007).
[7] C. Sönnichsen, T. Franzl, T. Wilk, G. von Plessen, and J. Feldmann, New J. Phys. **4**, 93 (2002).
[8] C. Sönnichsen, T. Franzl, T. Wilk, G. von Plessen, J. Feldmann, O. Wilson, and P. Mulvaney, Phys. Rev. Lett. **88**, 077402 (2002).
[9] U. Kreibig and M. Vollmer, Optical properties of metal clusters (Springer, Berlin, 1995).
[10] U. Kreibig, Appl. Phys. B-Lasers Opt. **93**, 79–89 (2008).
[11] B. Lamprecht, A. Leitner, and F. R. Aussenegg, Appl. Phys. B-Lasers Opt. **68**, 419–423 (1999).
[12] B. Lamprecht, J. R. Krenn, A. Leitner, and F. R. Aussenegg, Phys. Rev. Lett. **83**, 4421–4424 (1999).

Original Paper

[13] M. G. Blaber, A. I. Henry, J. M. Bingham, G. C. Schatz, and R. P. Van Duyne, J. Phys. Chem. C **116**, 393–403 (2012).

[14] T. G. Habteyes, S. Dhuey, S. Cabrini, P. J. Schuck, and S. R. Leone, Nano Lett. **11**, 1819–1825 (2011).

[15] C. Voisin, N. Del Fatti, D. Christofilos, and F. Vallée, J. Phys. Chem. B **105**, 2264–2280 (2001).

[16] J. Köhn and T. Fennel, Phys. Chem. Chem. Phys. **13**, 8747–8754 (2011).

[17] G. Sansone, E. Benedetti, F. Calegari, C. Vozzi, L. Avaldi, R. Flammini, L. Poletto, P. Villoresi, C. Altucci, R. Velotta, S. Stagira, S. De Silvestri, and M. Nisoli, Science **314**, 443–446 (2006).

[18] H. Mashiko, M. J. Bell, A. R. Beck, M. J. Abel, P. M. Nagel, C. P. Steiner, J. Robinson, D. M. Neumark, and S. R. Leone, Opt. Express **18**, 25887–25895 (2010).

[19] E. Goulielmakis, Z. H. Loh, A. Wirth, R. Santra, N. Rohringer, V. S. Yakovlev, S. Zherebtsov, T. Pfeifer, A. M. Azzeer, M. F. Kling, S. R. Leone, and F. Krausz, Nature **466**, 739–743 (2010).

[20] X. M. Feng, S. Gilbertson, H. Mashiko, H. Wang, S. D. Khan, M. Chini, Y. Wu, K. Zhao, and Z. H. Chang, Phys. Rev. Lett. **103**, 183901 (2009).

[21] A. L. Cavalieri, N. Müller, T. Uphues, V. S. Yakovlev, A. Baltuška, B. Horvath, B. Schmidt, L. Blümel, R. Holzwarth, S. Hendel, M. Drescher, U. Kleineberg, P. M. Echenique, R. Kienberger, F. Krausz, and U. Heinzmann, Nature **449**, 1029–1032 (2007).

[22] E. Goulielmakis, M. Uiberacker, R. Kienberger, A. Baltuška, V. Yakovlev, A. Scrinzi, T. Westerwalbesloh, U. Kleineberg, U. Heinzmann, M. Drescher, and F. Krausz, Science **305**, 1267–1269 (2004).

[23] S. Zherebtsov, T. Fennel, J. Plenge, E. Antonsson, I. Znakovskaya, A. Wirth, O. Herrwerth, F. Sussmann, C. Peltz, I. Ahmad, S. A. Trushin, V. Pervak, S. Karsch, M. J. J. Vrakking, B. Langer, C. Graf, M. I. Stockman, F. Krausz, E. Ruhl, and M. F. Kling, Nat. Phys. **7**, 656–662 (2011).

[24] S. Nagele, R. Pazourek, J. Feist, K. Doblhoff-Dier, C. Lemell, K. Tőkési, and J. Burgdörfer, J. Phys. B-At. Mol. Opt. Phys. **44**, 081001 (2011).

[25] E. E. Krasovskii, Phys. Rev. B **84**, 195106 (2011).

[26] C. H. Zhang and U. Thumm, Phys. Rev. A **84**, 033401 (2011).

[27] C. H. Zhang and U. Thumm, Phys. Rev. A **84**, 063403 (2011).

[28] P. M. Nagel, J. S. Robinson, B. Harteneck, T. Pfeifer, M. J. Abel, J. S. Prell, D. M. Neumark, R. A. Kaindl, and S. R. Leone, Chem. Phys. doi:10.1016/j.chemphys.2012.03.013 (2012).

[29] T. Pfeifer, M. J. Abel, P. M. Nagel, A. Jullien, Z. H. Loh, M. J. Bell, D. M. Neumark, and S. R. Leone, Chem. Phys. Lett. **463**, 11–24 (2008).

[30] M. I. Stockman, M. F. Kling, U. Kleineberg, and F. Krausz, Nat. Photonics **1**, 539–544 (2007).

[31] F. Süßmann and M. F. Kling, Phys. Rev. B **84**, 121406(R) (2011).

[32] E. Skopalová, D. Y. Lei, T. Witting, C. Arrell, F. Frank, Y. Sonnefraud, S. A. Maier, J. W. G. Tisch, and J. P. Marangos, New J. Phys. **13**, 083003 (2011).

[33] A. T. J. B. Eppink and D. H. Parker, Rev. Sci. Instrum. **68**, 3477–3484 (1997).

[34] M. Meier and A. Wokaun, Opt. Lett. **8**, 581–583 (1983).

[35] E. D. Palik (ed.), Handbook of Optical Constants of Solids (Elsevier, 1998).

[36] J. D. Jackson, Classical Electrodynamics (Wiley, New York, 1999).

[37] M. P. Seah and W. A. Dench, Surf. Interface Anal. **1**, 2–11 (1979).

[38] K. R. Wilson, S. L. Zou, J. N. Shu, E. Rühl, S. R. Leone, G. C. Schatz, and M. Ahmed, Nano Lett. **7**, 2014–2019 (2007).

[39] S. Zherebtsov, A. Wirth, T. Uphues, I. Znakovskaya, O. Herrwerth, J. Gagnon, M. Korbman, V. S. Yakovlev, M. J. J. Vrakking, M. Drescher, and M. F. Kling, J. Phys. B-At. Mol. Opt. Phys. **44**, 105601 (2011).